Vibrational and Photochemical Consequences of an Asp Residue Near the Photoactive Accessory Bacteriochorophyll in the Photosynthetic Reaction Center†

Kazimierz Czarnecki,‡ Christine Kirmaier,§ Dewey Holten,§ and David F. Bocian*,‡

Department of Chemistry, University of California, Riverside, California 92521-0403, and Department of Chemistry, Washington University, St. Louis, Missouri 63130-4899

Received: August 27, 1998

Q_y-excitation resonance Raman (RR) and subpicosecond resolution transient absorption (TA) studies are reported for *Rhodobacter capsulatus* reaction centers (RCs) containing a mutation at M-polypeptide residue 201 near the photoactive accessory bacteriochlorophyll ($BChl_L$). The studies focus on the electronic/vibrational perturbations induced by replacing the native Gly with an Asp residue and examine the effects of temperature on these perturbations. The RCs include the G(M201)D single and G(M201)D/L(M212)H double mutants. In the double mutant, a BChl molecule (designated β) replaces the native photoactive bacteriopheophytin (BPh_L). Analysis of the crystal structure coordinates of the RC indicates that the oxygens of the carbonyl group of the Asp at position M201 should be within a few angstroms of the oxygen of the C_9-keto group of $BChl_L$. RR studies on both the G(M201)D and G(M201)D/L(M212)H RCs at room temperature indicate that replacing Gly at position M201 with Asp significantly perturbs the vibrational characteristics of $BChl_L$, and in a manner most consistent with Asp M201 being deprotonated and negatively charged. The negative charge of the carboxyl group of Asp M201 interacts with the π-electron system of $BChl_L$ in a relatively nonspecific fashion, diminishing the contribution of charge-separated resonance forms of the C_9-keto group to the electronic structure of the cofactor. The RR results are consistent with the effects of Asp M201 on the primary photochemistry found in earlier TA studies on G(M201)D/L(M212)H RCs, which indicate that the Asp residue raises the free energy of state $P^+BChl_L^-$ (Heller et al. *Science* **1995**, *269*, 940−945). The interactions between the C_9-keto group of $BChl_L$ and the carboxyl of Asp M201 are different at ambient versus low temperatures, as reflected in both the RR spectra and TA data on G(M201)D and G(M201)D/L(M212)H RCs. In particular, as the temperature is reduced, both the vibrational characteristics of $BChl_L$ and the primary photochemistry in the two mutants become more like those found in RCs without the G(M201)D mutation.

Introduction

The reaction center (RC) is a membrane-bound protein responsible for the initial stages of the photoconversion process in photosynthesis.[1] Purple bacterial RCs contain four bacteriochlorophylls (BChls), two bacteriopheophytins (BPhs), two quinones (Q), a non-heme iron, and a carotenoid arranged in three polypeptide subunits designated L, M, and H. Two of the BChl molecules form a dimer (P). The X-ray crystal structures of RCs from two purple bacteria (*Rhodobacter sphaeroides* and *Rhodopseudomonas viridis*) reveal that P, the accessory BChls, and the BPhs are arranged in the L and M subunits such that the macroscopic symmetry is approximately C_2 (Figure 1).[2] The detailed structure of BChl is shown in Figure 2; BPh differs from BChl in the replacement of the central Mg^{2+} ion by two protons. Upon excitation, P is elevated to its excited singlet state (P*), which transfers an electron in about 3 ps to the BPh molecule associated with the L polypeptide (BPh_L) (Figure 3A). This process utilizes the BChl cofactor on the L branch ($BChl_L$) as a discrete intermediate, a superexchange mediator, or both. Subsequently, $BPhL^-$ transfers an electron in about 200 ps to its neighboring quinone (Q_A). The quantum yield of the overall process is approximately unity.

The relative free energies of P*, $P^+BChl_L^-$, and $P^+BPh_L^-$ are critical in determining the rates and yields of the formation and decay pathways of $P^+BPh_L^-$. Furthermore, because the total free-energy span encompassing these states is less than 300 meV, modest changes in the free energies can have dramatic

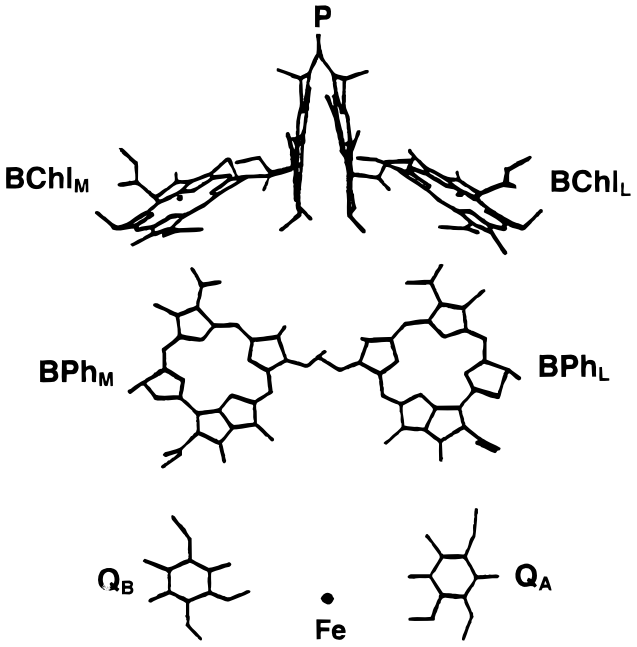

Figure 1. Schematic structure of the bacterial RC showing the arrangement of the cofactors.

† Dedicated to the memory of Bryan E. Kohler, 1940−1997.
‡ University of California.
§ Washington University.

10.1021/jp983558q CCC: $18.00
Published on Web 01/09/1999

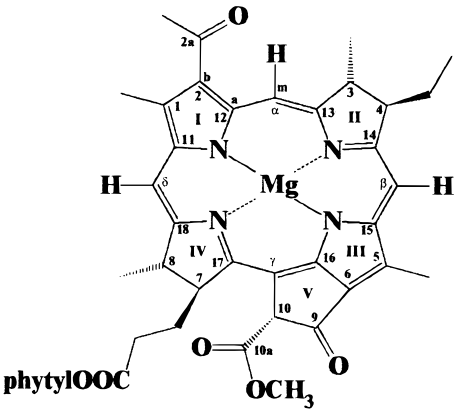

Figure 2. Structure and labeling scheme for BChl a.

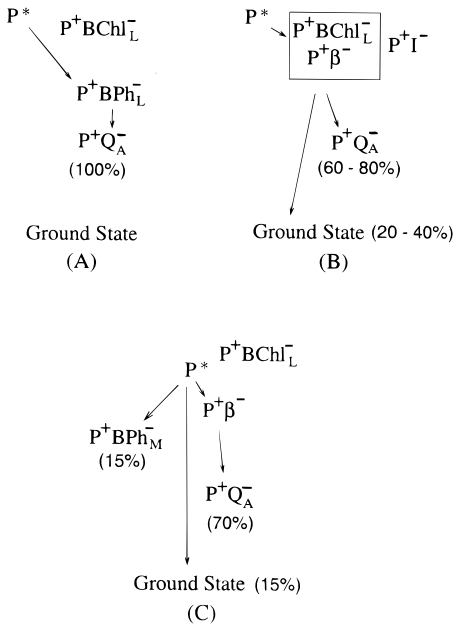

Figure 3. Summary state diagrams for the primary photochemistry in (A) wild-type RCs, (B) beta-type single mutants such as L(M212)H in which BPh_L is replaced with a BChl (β), and (C) the G(M201)D/L(M212)H double mutant. Note that the values given in (B) cover a series of beta-type mutants from *Rb. capsulatus* and *Rb. sphaeroides*, and similar characteristics apply to the F(L121)D mutant, which retains the native pigment content. Note also that potential small (<10%) yields of other processes such as formation of $P^+BPh_M^-$ from P* in the RCs in (A) or (B) or decay of the nominal $P^+\beta^-$ state to the ground state in (C) are not shown for clarity.

consequences. This point has been demonstrated in RCs in which BPh_L is replaced either by a BChl designated β (a result of genetic incorporation of a His residue over the cofactor)[3] or by another tetrapyrrole (accomplished by chemical substitution).[4] In both the beta-type and chemically modified RCs, P* decays with a somewhat longer lifetime than in wild-type RCs to give a P^+I^- transient from which electron transfer to Q_A proceeds with a diminished overall yield of $P^+Q_A^-$ (Figure 3B). The diminished yield is ascribed to increased involvement of $P^+BChl_L^-$ in P^+I^-, which results in (1) substantially faster charge recombination to the ground state (due to the shorter distance between the hole on P^+ and electron density on $BChl_L^-$ versus BPh_L^- (or β^-)) and (2) somewhat slower electron transfer to Q_A (due to the longer distance to this cofactor from $BChl_L^-$ versus BPh_L^- (or β^-)). The increased involvement of $P^+BChl_L^-$ in beta-type RCs arises because $P^+\beta^-$ is at a higher free energy than $P^+BPh_L^-$, owing to the more negative reduction potential of BChl versus BPh.[5] (Analogous arguments apply to chemically

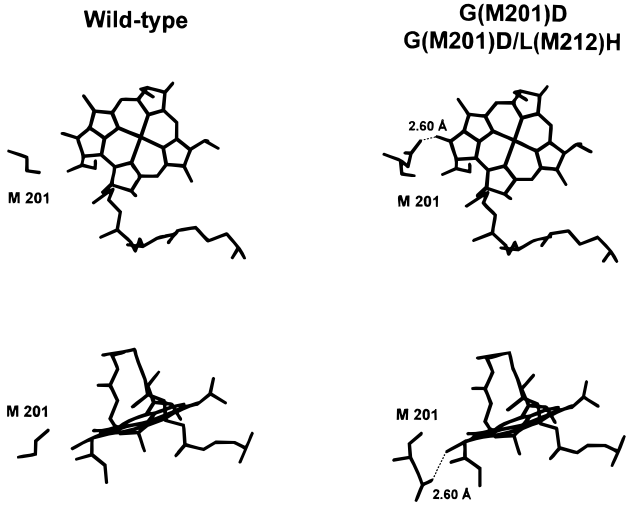

Figure 4. Two views of $BChl_L$ showing the locations of residue Gly M201 in wild-type RCs (left panel) and two views of $BChl_L$ with an Asp residue substituted at position M201 (right panel). In these latter views, the Asp has been positioned by simple replacement of the native Gly residue in the crystal structure. In both views, the phytyl substituent of $BChl_L$ has been removed for clarity. The figure was constructed using the X-ray crystallographic data for *Rb. sphaeroides* RCs[2a] because X-ray data is not available for *Rb. capsulatus* RCs.

modified RCs.[4a]) Consequently, P^+I^- is best characterized as a thermal/quantum admixture of $P^+BChl_L^-$ and $P^+\beta^-$.[3d,e]

The incorporation of Asp residues in proximity to ring V of the BChl/BPh cofactors has been shown to influence the charge-separation process, in some cases in a quite remarkable manner.[3e,6,7] For example, we recently showed that the F(L121)D mutant (where an Asp replaces the native Phe at position L121, near ring V of BPh_L[2]) exhibits beta-type photochemistry (analogous to that depicted in Figure 3B) while maintaining a normal pigment composition.[7] We ascribed this to a higher free energy of $P^+BPh_L^-$ (and consequent increased involvement of $P^+BChl_L^-$ in the decay of this state) in the F(L121)D mutant relative to wild-type RCs, similar to the higher free energy of $P^+\beta^-$ in the L(M212)H mutant (see Figure 3B). Along similar lines, replacing the native Gly residue at position M201 (near the edge of ring V of $BChl_L$[2]) with an Asp residue in the beta-type template, giving the G(M201)D/L(M212)H double mutant, substantially raises the free energy of $P^+BChl_L^-$. This increase occurs to such an extent that the formation/decay kinetics and yields of the L-branch intermediates are modified and a low (~15%) yield of electron transfer is observed down the normally inactive M-branch (Figure 3C).[3e] The position of Gly M201 is illustrated schematically in Figure 4 (left panel). Simple replacement of Gly with Asp in the crystal-structure coordinates yields a distance of closest approach between the oxygens of the carboxyl group of Asp M201 and the oxygen of the C_9-keto group of $BChl_L$ of ~2.6 Å, as is illustrated schematically in Figure 4 (right panel).

On the basis of modeling of the changes in the primary photochemistry, the effects of the Asp residues on the free energies of $P^+BPh_L^-$ in F(L121)D RCs and $P^+BChl_L^-$ in G(M201)D/L(M212)H RCs are estimated to be very large (up to ~175 meV).[3e,7] These effects are significantly larger than the changes that have been elicited by adding or removing single hydrogen bonds (~60 meV) to a chromophore.[3d,8,9] As a consequence, the simplest (but not exclusive) interpretation is that the Asp residue in both the F(L121)D and G(M201)D/L(M212)H RCs mutants is deprotonated and negatively charged.[3e,7] This view is supported by our recent resonance Raman (RR) studies on F(L121)D RCs that probed the effects of the Asp residue on the vibrational characteristics of the ring-skeletal and carbonyl modes of BPh_L.[10]

Herein, we report the results of RR and transient absorption (TA) studies of the *Rb. capsulatus* G(M201)D single mutant and G(M201)D/L(M212)H double mutant. The RR studies focus on the vibrational characteristics of the $BChl_L$ cofactor. The RR data were acquired using excitation into the red-most Q_y absorption bands of the BChl cofactors. Q_y excitation (as opposed to Q_x or B excitation) was chosen both to facilitate RR enhancement of the vibrations of the BChls over those of the BPhs and P and to maximize enhancement of the keto modes of the chromophores.[11−13] Q_y excitation maximizes enhancement of the keto vibrations because the keto groups lie along the *y* axis of the tetrapyrrole macrocycle. The effects of temperature on the vibrational characteristics of the BChls and on the photochemical processes in the mutants were also examined in parallel. Collectively, the RR and TA data provide further insights into the protonation/charge state of the Asp residue and the consequent effects on the properties of $BChl_L$ and, ultimately, on the charge-separation process in these mutants.

Materials and Methods

Sample Preparation. The *Rb. capsulatus* wild-type, G(M201)D, and G(M201)D/L(M212)H RCs were prepared, isolated, and purified as previously described.[3b,e,7] Note that the secondary quinone (Q_B) is not present (<10%) in these RCs. The RCs for RR measurements were solubilized in 10 mM Tris-HCl (pH 8)/0.1% triton X-100/1 mM EDTA, and Q_A was reduced by addition of a slight excess of buffered sodium dithionite solution. Samples for TA studies were suspended in 10 mM potassium phosphate (pH 7.6)/0.05% *N*,*N*-dimethyldodecylamine *N*-oxide (LDAO)/1 mM EDTA.

RR Measurements. The RR measurements were made on optically dense (OD, ∼1.0/mm at 800 nm; RC concentration, ∼35 μM) samples contained in 1 mm i.d. capillary tubes. For the studies at all temperatures, the samples (in neat buffer) were mounted on the cold tip of a closed cycle refrigeration system (ADP Cryogenics, DE-202 Displex). The advantages and disadvantages of using snowy versus glassy samples have been previously discussed.[12b]

The RR spectra were obtained using a red-optimized triple spectrograph and a detection system that has been previously described.[12a] A Ti:sapphire laser (Coherent 890) pumped by an Ar ion laser (Coherent Innova 400-15UV) served as the excitation source. The laser powers were typically 1.0−1.5 mW. The power density on the sample was adjusted by defocusing the incident laser beam. The resulting photon fluxes (∼100 photons s^{-1} RC^{-1}) were low enough that, in steady state, only a few percent of the RCs existed in photogenerated transient states. Each RR data set was obtained with 3−4 h of signal averaging. The data acquisition time for an individual scan was dictated by the level of background fluorescence from a particular sample (vide infra). These times ranged from 20−50 s for the different RCs. Cosmic spikes in the individual scans were removed prior to coaddition of the scans. The spectral resolution was ∼2 cm^{-1} in all spectral regions. The spectral data were calibrated using the frequencies of fenchone.[14]

The Q_y-excitation RR spectra for all three RCs were superimposed on an emission background. The fluorescence background was particularly large in the region of the high-frequency modes (1600−1750 cm^{-1}), which are the principal focus of this study. The fluorescence background, in conjunction with the fact that the Q_y-excitation RR intensity enhancements of the high-frequency modes of BChl are generally weak,[12a,13d,15] compromise the quality of the spectra. Therefore, all the RR spectra were acquired using the shifted-excitation Raman difference spectroscopic (SERDS) technique.[13a,16] The application of the SERDS method to RCs has been previously described in detail.[12b−f,13] Briefly, each data set is acquired at two excitation wavelengths that differ by a small wavenumber increment (typically 10 cm^{-1}). (The 3−4 h data acquisition time indicated above is for each of the two data sets required to construct a given SERDS trace.) These data sets are subtracted to yield a background-free RR difference (SERDS) spectrum. The RR spectra presented herein were obtained by subtracting the initial spectrum from the shifted spectrum. The spectral window is defined by the initial spectrum and corresponds to the wavenumber axis in the figures. The normal RR spectrum is then reconstructed from the SERDS data by fitting the latter to a series of derivative-shaped functions (in this case difference bands generated from Gaussian functions) of arbitrary frequency, amplitude, and width. The frequencies marked in the figures correspond to the positions of the bands used in the fits and, thus, do not necessarily correspond to the peak maxima for overlapping bands. In addition, certain bands are marked that are not clearly resolved in the spectra. These bands are indicated because their inclusion noticeably improved the quality of the fits to the SERDS data.

TA Measurements. The TA studies utilized 100−200 fs excitation flashes at 582 nm from an amplified synchronously pumped dye laser system or 850 nm from an amplified Ti:sapphire laser system. In both cases, the excitation flashes were attenuated to excite ≤25% of the RCs.[3e,17] For the studies at 285 K, the RCs were flowed through a 2 mm path length cell (A_{800} = 0.7 or 2 for measurements at >730 nm or <730 nm, respectively) and were excited at 10 Hz. For the studies at 77 K, static samples (in 60/40 v/v glycerol/buffer) were housed in an Oxford Instruments cryostat and were excited at 5 Hz. Note that even at this relatively low repetition rate a small amount of P bleaching was observed before the pump−probe zero time. The magnitude of this pre-zero-time bleaching was ∼15% of that observed after zero time and corresponds to a residual steady-state fraction of RCs remaining in the charge-separated state (e.g., $P^+Q_A^-$) between the arrival of excitation pulses at 5 Hz. A slightly larger pre-zero-time bleaching was observed at 77 K at 10 Hz. However, the relative amplitudes of the transient absorption spectra obtained at various delay times were the same at the two repetition rates after correcting for (ie., subtracting) the pre-zero-time signals. (We note that the spectral data shown in Figures 9 and 10 have had the pre-zero-time spectra subtracted from that shown at the given delay times.) We also collected kinetic data at both 5 and 10 Hz and found no effects on the measured lifetimes. These findings indicate that the reported lifetimes and relative state yields should not differ significantly (if at all) from those that would be observed if complete recovery had occurred between the excitation flashes.

Results

RR Spectra. The high-frequency regions (1375−1750 cm^{-1}) of the Q_y-excitation RR spectra of *Rb. capsulatus* wild-type (λ_{ex} = 800 nm), G(M201)D (λ_{ex} = 795 nm), and G(M201)D/L(M212)H (λ_{ex} = 795 nm) RCs obtained at 277 K and at 25 K are shown in Figures 5 and 6, respectively. In both figures, the top trace in each panel is the raw (unsmoothed) SERDS data, the second trace is the fit of the SERDS data, the third trace is the SERDS residual (observed minus fit), and the bottom trace is the RR spectrum reconstructed from the SERDS data. The relatively small residuals compared with the SERDS intensities are indicative of the excellent fidelity of the fits. To facilitate

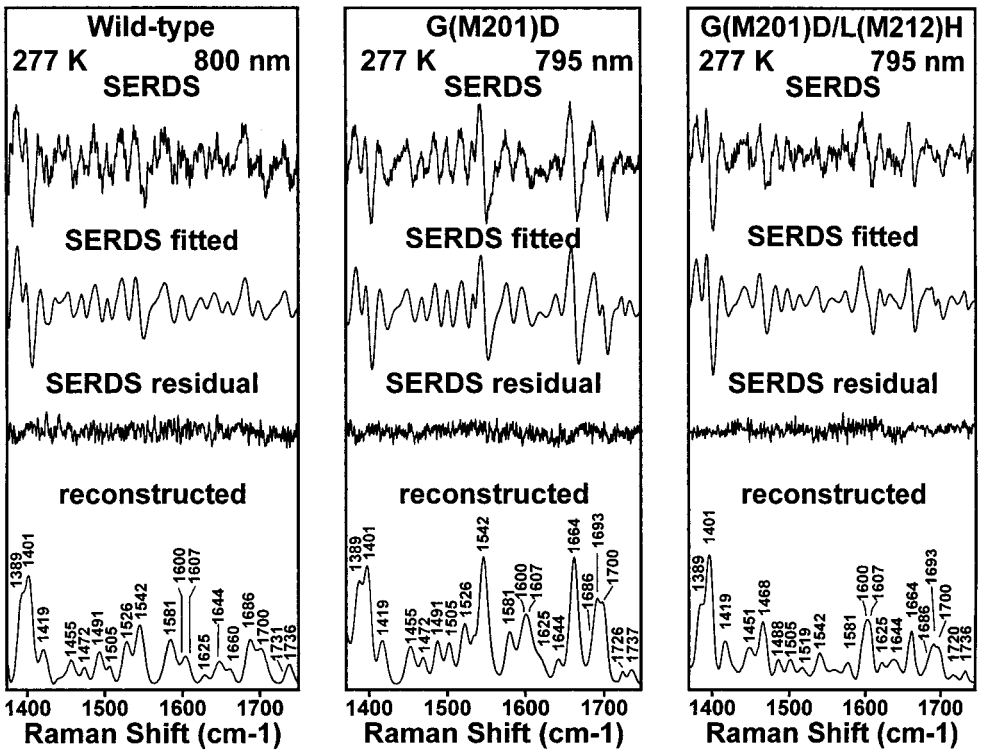

Figure 5. Q_y-excitation RR spectra of the BChls of wild-type (λ_{ex} = 800 nm), G(M201)D (λ_{ex} = 795 nm), and G(M201)D/L(M212)H (λ_{ex} = 795 nm) RCs obtained at 277 K. In each panel, the top trace is the SERDS data, the second trace is the fit of the SERDS data, the third trace is the SERDS residual (observed−fit), and the bottom trace is the RR spectrum reconstructed from the SERDS data.

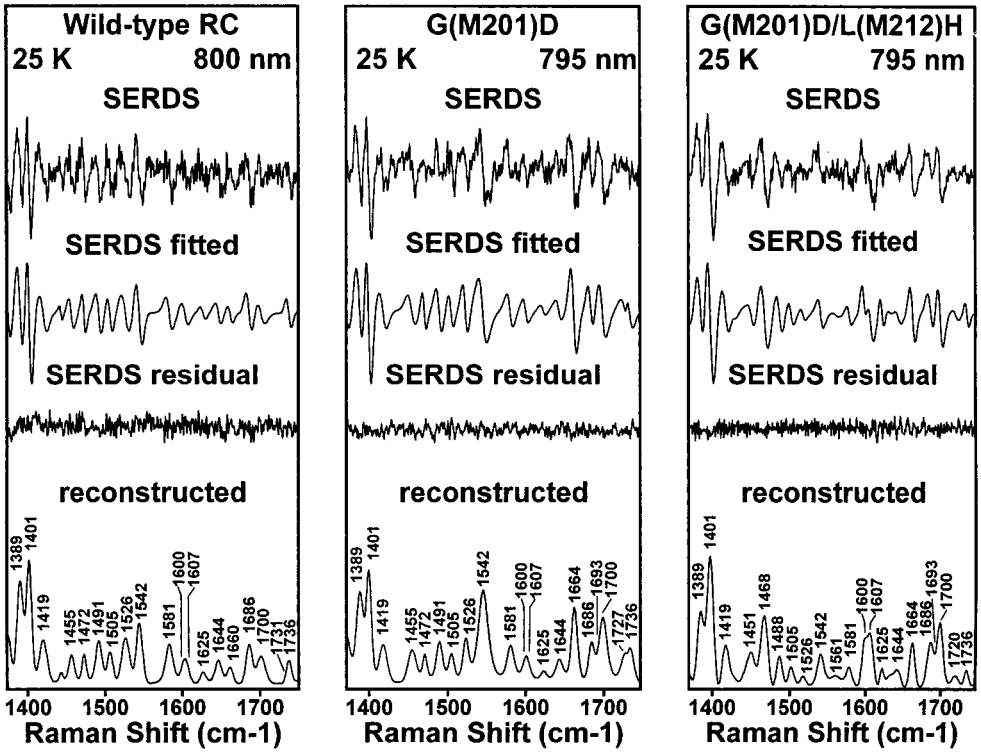

Figure 6. Q_y-excitation RR spectra of the BChls of wild-type (λ_{ex} = 800 nm), G(M201)D (λ_{ex} = 795 nm), and G(M201)D/L(M212)H (λ_{ex} = 795 nm) RCs obtained at 25 K. In each panel, the top trace is the SERDS data, the second trace is the fit of the SERDS data, the third trace is the SERDS residual (observed−fit), and the bottom trace is the RR spectrum reconstructed from the SERDS data.

comparison, the reconstructed RR spectra for the three different RCs obtained at 277 and 25 K are reproduced on an expanded scale in Figure 7. This spectral window encompasses the region of the carbonyl and certain ring-skeletal stretching modes of the BChls. The temperature dependence of the RR scattering characteristics of the carbonyl and high-frequency ring-skeletal modes of the BChls in G(M201)D RCs is shown in Figure 8. (Note that certain RR features are labeled in Figures 7 and 8 that are not labeled in Figures 5 and 6 for pictorial clarity.)

In addition to the spectra obtained with the excitation wavelengths indicated in Figures 5−7, RR spectra were also obtained at selected other excitation wavelengths in the 790−

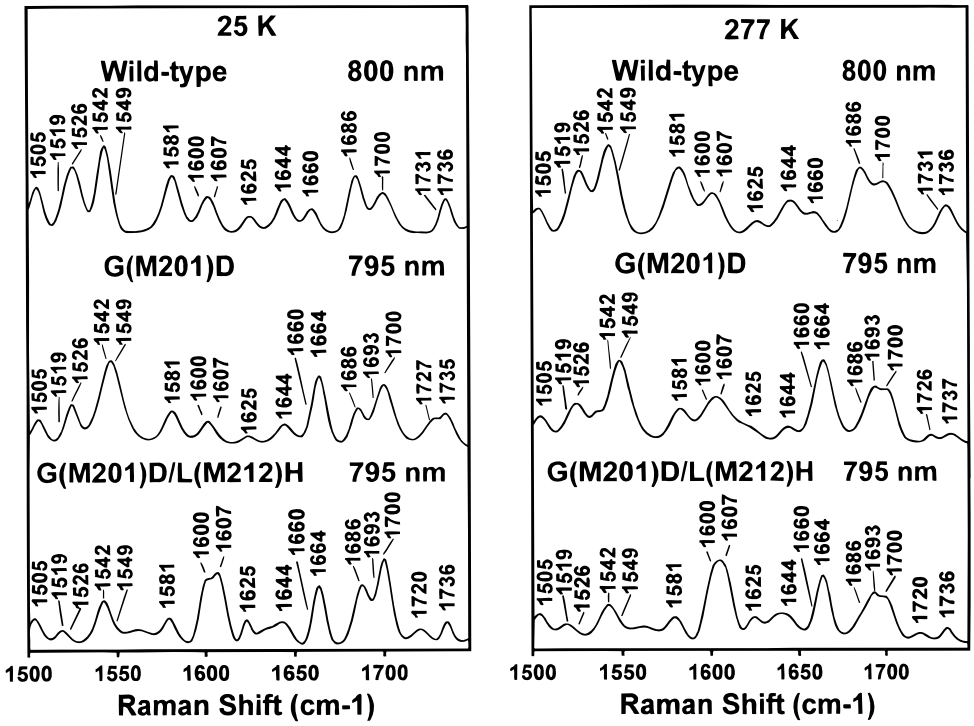

Figure 7. Comparison of the Q_y-excitation RR spectra of the BChls of wild-type, G(M201)D, and G(M201)D/L(M212)H RCs in the region of the carbonyl and high- frequency ring-skeletal stretching modes (277 K, right panel; 25 K, left panel). The data are the same as those of the bottom traces of Figures 5 and 6.

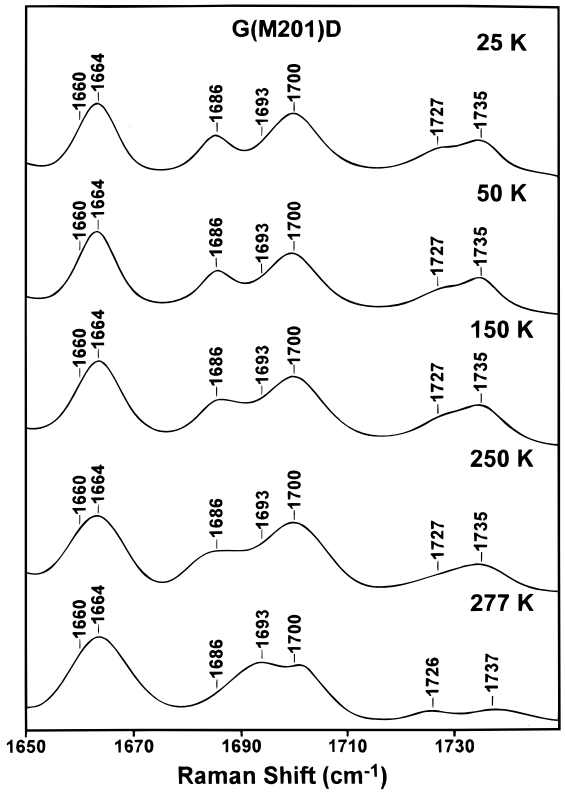

Figure 8. Temperature dependence of the Q_y-excitation RR spectra of the BChls in G(M201)D RCs.

810 nm region (not shown). These spectra do not reveal any additional features. Excitation in the 790−810 nm region elicits RR scattering exclusively from the BChls.[12a] For the G(M201)D/L(M212)H RCs, RR spectra were also recorded with excitation at $\lambda_{ex} = 775$ nm. This excitation wavelength probes the β cofactor in these RCs.[12e] The RR scattering characteristics of this cofactor were found to be identical to those of the β cofactor in RCs from the *Rb. capsulatus* L(M212)H single mutant (Czarnecki, K.; Bocian, D. F., unpublished results). The RR scattering characteristics of the β cofactors in RCs from both the *Rb. capsulatus* L(M212)H and G(M201)D/L(M212)H mutants were also found to be very similar to those we have previously reported for the analogous *Rb. sphaeroides* L(M214)H single mutant.[12e] For this reason and because the β cofactor is not the focus of the present study, the reader is referred to our previous work on the L(M214)H RCs for a detailed discussion of the RR scattering characteristics of the β cofactor.

Inspection of Figure 7 reveals that many of the general features of the RR spectra of the different genetically modified RCs are similar to one another and similar to those of wild-type RCs. For each of the RCs, the vibrations enhanced with Q_y excitation include the stretching modes of the C_{10a}-carbomethoxy (1730−1740 cm^{-1}), C_9-keto (1685−1695 cm^{-1}), and C_{2a}-acetyl (1660−1665 cm^{-1}) carbonyl groups. Two additional bands in this general spectral region (at 1700 and ∼1725 cm^{-1}) are not νC═O vibrations but are most likely combination modes.[10,12a,18] Q_y excitation also enhances the ring stretching modes of the C_aC_m and unsaturated C_bC_b bonds (1500−1650 cm^{-1}).[11,12a] The remaining stretching modes of the C_aC_m bonds as well as those of the C_aC_b and C_aN bonds occur at lower frequencies (1300−1500 cm^{-1}; see Figures 5 and 6).[12a]

The focus of the present study is on differences in the frequencies of analogous RR bands of $BChl_L$ in the various RCs (and their positions relative to those of $BChl_M$) and not on differences in relative RR intensities. The frequencies of the RR bands are of particular interest because these features reflect the properties of the ground electronic states of the cofactors. In contrast, the RR intensities are strongly affected by the properties of the Q_y excited states of the chromophores (via origin shifts and/or dephasing times of certain modes). These excited-state properties are outside the scope of this paper.

TABLE 1: RR Frequencies (cm^{-1})[a] and Assignments[b] for the Carbonyl and Selected Ring-Skeletal Modes of $BChl_L$ and $BChl_M$[c]

	wild type		G(M201)D		G(M201)D/ L(M212)H	
description[d]	$BChl_L$	$BChl_M$	$BChl_L$	$BChl_M$	$BChl_L$	$BChl_M$
νC_{10a}=O	1736		1737		1736	
νC_9=O	1686		1693	1686	1693	1686
νC_{2a}=O	1660		1664	1660[e]	1664	1660[e]
$[\nu C_aC_m(\gamma),\nu C_9$=O]	1644		1644		1644	
$[\nu C_bC_b(III),\nu C_aC_m(\gamma)]$	1625		1625		1625	
$\nu C_aC_m(\alpha,\beta,\gamma,\delta)$	1607		1607		1607	
$[\nu C_aC_m(\delta),\nu C_bC_b(I)]$	1600		1600		1600	

[a] Frequencies are for data acquired at 277 K. [b] Taken from ref 12a. [c] A single frequency indicates that the bands for $BChl_L$ and $BChl_M$ are coincident. [d] The designations C_a, C_b, C_m, III, α, β, γ, δ refer to Figure 2. [e] This band is masked by the more intense 1664 cm^{-1} band (see text).

Nonetheless, it should be noted that the RR intensity differences that are observed upon replacement of the native Gly M201 with Asp derive largely if not exclusively from electronic perturbations to the Q_y excited state of $BChl_L$. This follows from the fact that the (ground-state) vibrational frequencies are generally quite similar (with certain exceptions (vide infra)) for wild-type, G(M201)D, and G(M201)D/L(M212)H RCs. On the other hand, the replacement of Gly M201 with Asp causes the $Q_y(0,0)$ band of $BChl_L$ to slightly blue shift.[6,7] In the case of the G(M201)D/L(M212)H RCs, the presence of the β cofactor probably causes additional perturbations on the Q_y excited state of $BChl_L$,[3a,c,7] including some degree of quantum admixing with the Q_y excited state of β. These differences in the Q_y excited-state properties of $BChl_L$ among the wild-type, G(M201)D, and G(M201)D/L(M212)H RCs most likely all contribute to the RR intensity differences observed for certain bands of $BChl_L$ relative to other bands of this cofactor (and with respect to those of $BChl_M$).

The fact that the RR frequencies of the BChl cofactors of the various genetically modified RCs are generally similar to one another and similar to those of wild-type RCs permits assignment of the vibrational modes of the mutants by direct analogy to those previously reported for wild-type RCs.[12a] The overall rationale for the vibrational assignments of the BChls has been previously discussed in detail and will not be reiterated here. Although these earlier vibrational assignments were made for *Rb. sphaeroides* rather than *Rb. capsulatus* wild-type RCs,[12a] RR studies have shown that the spectral signatures of these two different wild-type RCs are quite similar.[19]

The frequencies and normal-mode descriptions of the RR bands in the 1600−1750 cm^{-1} region that are assigned to fundamental carbonyl or ring-skeletal vibrations of the BChls are summarized in Table 1. One key feature of the vibrational assignments for the BChls in wild-type RCs is that the frequencies of analogous modes of $BChl_L$ and $BChl_M$ are very close and cannot be resolved in the RR spectra.[12a,b,13b] Consequently, these modes of the two cofactors of wild-type RCs hereafter will be designated collectively as $BChl_{L,M}$. In the sections below, we first describe the specific RR scattering characteristics of the various types of modes of the different RCs. This analysis focuses on the features observed at near-ambient temperature (Figure 5 and Figure 7 (right panel)). We then examine the features observed at low temperature (Figure 6 and Figure 7 (left panel)) as well as a function of temperature (Figures 7 and 8).

Carbonyl Modes. The wild-type *Rb. capsulatus* RCs exhibit RR bands at 1736, 1686, and 1660 cm^{-1} (Figure 7 (right panel); Table 1) that are attributed to the νC_{10a}=O, νC_9=O, and νC_{2a}=O, of $BChl_{L,M}$, respectively.[12a,20] These frequencies indicate that all three keto groups of both BChls are free of hydrogen bonds. This is also the case for the keto groups of the BChls of wild-type *Rb. sphaeroides* RCs.[21] The effect of the G(M201)D mutation in both the single and double Asp mutants is most pronounced on the νC_9=O vibration, whereas the effects on the νC_{10a}=O and νC_{2a}=O modes are modest to negligible.

The specific observations for the νC=O vibrations of the BChls for the different RCs at 277 K are as follows. (1) In the region of the νC_9=O modes (1685−1695 cm^{-1}), both mutants exhibit a 1693/1686 cm^{-1} pair of bands compared with the single 1686 cm^{-1} band of the wild-type. The 1686 cm^{-1} band is seen as a clear shoulder on the 1693 cm^{-1} band in the double mutant, somewhat less so in the single mutant. The presence of the 1686 cm^{-1} band is further indicated by the spectral simulations, which show that the data for the wild-type RCs can be fit with two bands (1686 and 1700 cm^{-1}) of equal width whereas three bands (1686, 1693, and 1700 cm^{-1}) of the same width must be used to fit the data for the two mutant RCs. (2) In the region of the νC_{2a}=O vibrations (1660−1665 cm^{-1}), both mutants exhibit a 1664/1660 cm^{-1} pair of bands compared with the single 1660 cm^{-1} band of the wild-type. The relatively weak 1660 cm^{-1} band is nearly completely masked by its much stronger 1664 cm^{-1} partner. Nevertheless, the spectral simulations again indicate that a better fit of the data is obtained by including the former. (3) In the region of the νC_{10a}=O vibrations (1730−1740 cm^{-1}), both the G(M201)D and G(M201)D/L(M212)H RCs exhibit a single ~1737 cm^{-1} band, similar to the single 1736 cm^{-1} band of wild-type RCs. The most straightforward explanation for all of the above noted observations for the G(M201)D and G(M201)D/L(M212)H RCs is that the shifted (relative to wild-type) νC_9=O and νC_{2a}=O RR bands are due to $BChl_L$, whereas the unshifted bands are due to $BChl_M$ (Table 1).

Ring-Skeletal Modes. The wild-type (and mutant) RCs exhibit at least 10 RR bands in the 1500−1650 cm^{-1} region that are assigned to ring-skeletal vibrations of $BChl_{L,M}$.[12a] Two bands of particular interest are observed near 1625 and 1607 cm^{-1} (Figure 7 (right panel); Table 1). The 1625 cm^{-1} vibration, $[\nu C_bC_b(III),\nu C_aC_m(\gamma)]$, is predominantly due to stretching of the unsaturated C_bC_b bond in ring III along with a smaller component involving stretching of the methine bridge in the ring III/V region of the cofactor.[12a,22] This mode has no analog in metalloporphyrins and occurs at a relatively high frequency owing to strain in the ring III/V region. The 1607 cm^{-1} vibration, $\nu C_aC_m(\alpha,\beta,\gamma,\delta)$, is characterized by the stretching of all four methine bridges and is the analog of the ν_{10} vibration of metalloporphyrins.[12a,22] The salient observation concerning the $[\nu C_bC_b(III),\nu C_aC_m(\gamma)]$ and $\nu C_aC_m(\alpha,\beta,\gamma,\delta)$ vibrations, and indeed all of the other ring-skeletal modes, is that the G(M201)D mutation has essentially no effect on their frequencies (Figures 5 and 7 (right panels); Table 1). Accordingly, the RR bands of the analogous ring-skeletal modes of the two BChls in the G(M201)D and G(M201)D/L(M212)H RCs are sufficiently close in frequency that they cannot be resolved, as is also the case for wild-type RCs.

Effects of Temperature. Inspection of Figure 7 reveals that the RR spectra of the wild-type RCs are essentially identical at 25 and 277 K. The only perceptible difference is that the RR bands at the lower temperature exhibit the expected spectral narrowing. The RR spectral features of the G(M201)D and G(M201)D/L(M212)H RCs are also largely insensitive to temperature, with one notable exception. For both mutants, the

general appearance of the composite band contour in the region of the νC_9═O modes (1685−1695 cm^{-1}) is quite different at 25 K compared with 277 K. At 25 K, the 1686 cm^{-1} band is very clearly resolved and there is little evidence of the 1693 cm^{-1} feature. In many respects, at 25 K, the band contour in this spectral region for the mutants appears to be much more similar to that of wild-type RCs than is the case at 277 K.

In order to better characterize the effects of temperature on the νC_9═O modes of the G(M201)D and G(M201)D/L(M212)H RCs, RR spectra were acquired at three additional temperatures between 25 and 277 K. The RR data shown for the G(M201)D RCs in Figure 8 are representative of the trends observed for both mutants. As is clearly seen in the figure, at 277 K, the peaks at 1693 and 1700 cm^{-1} are well resolved while the band at 1686 cm^{-1} is a shoulder. As the temperature is lowered, the band at 1686 cm^{-1} becomes increasingly well resolved while the peak at 1693 cm^{-1} diminishes; at 150 K and below, the feature at 1686 cm^{-1} is a clearly resolved band and the feature at 1693 cm^{-1} only fills in the contour between the bands at 1686 and 1700 cm^{-1}. Most of this change with temperature occurs between 277 K and the 150−50 K range; between 50 and 25 K, there are only minor changes in the shape of the band contour.

There are a variety of possible interpretations and qualifiers concerning precisely how temperature affects the peak intensities, widths, and frequencies of the bands near 1686 cm^{-1} (νC_9═O of $BChl_M$), 1693 cm^{-1} (νC_9═O of $BChl_L$), and 1700 cm^{-1} (combination mode). However, the most straightforward and consistent interpretation is that the decrease in the peak intensity of the 1693 cm^{-1} feature relative to those of the 1686 and 1700 cm^{-1} bands as the temperature is reduced arises from two main effects (Figure 8). These contributions are (i) an actual decrease in the integrated (absolute) intensity of the 1693 cm^{-1} band and (ii) an increase in the peak (but not integrated) intensities of the 1686 and 1700 cm^{-1} bands associated with the expected spectral narrowing (as occurs for all the other bands in the spectrum as the temperature is reduced).

It should be noted that although the νC_9═O mode of $BChl_L$ occurs at 1693 cm^{-1} at high temperature, where the peak is well resolved from the adjacent bands, the vibration may deviate somewhat from the 1693 cm^{-1} position indicated in the low-temperature RR spectra (Figures 6−8). However, the band does not simply disappear from the 1680−1720 cm^{-1} region at low temperature. Rather, it remains close (within ~5 cm^{-1}) to 1693 cm^{-1}, as indicated by the fit of the band contour in this spectral region, which requires the presence of a band between the 1686 and 1700 cm^{-1} features. Furthermore, interpretations involving simple broadening of the ~1693 and/or 1700 cm^{-1} bands as the temperature is reduced are inconsistent with the expected opposite band-narrowing effect for these features.

Thus, although a number of factors may contribute to the temperature dependence of the overall band contour in the 1680−1720 cm^{-1} region, it seems clear that bulk of the temperature dependence of the RR spectra of the G(M201)D and G(M201)D/L(M212)H mutants is exhibit by the ~1693 cm^{-1} νC_9═O mode of $BChl_L$. This observation, in conjunction with the fact that the analogous mode of $BChl_L$ in wild-type RCs is not affected by temperature, clearly indicates that some temperature-dependent property of Asp M201 is responsible for the behavior observed for the νC_9═O vibration of $BChl_L$ in the two mutants.

TA Spectra and Kinetics. TA measurements were performed on the G(M201)D/L(M212)H RCs at 77 K and, for comparison purposes, on the two single mutants G(M201)D and L(M212)H.

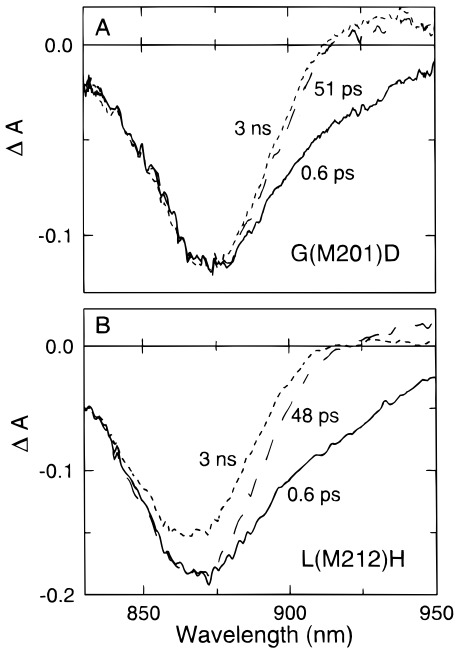

Figure 9. Representative near-infrared absorption difference spectra at 77 K acquired following a 150 fs flash at 580 nm for (A) G(M201)D RCs and (B) L(M212)H RCs.

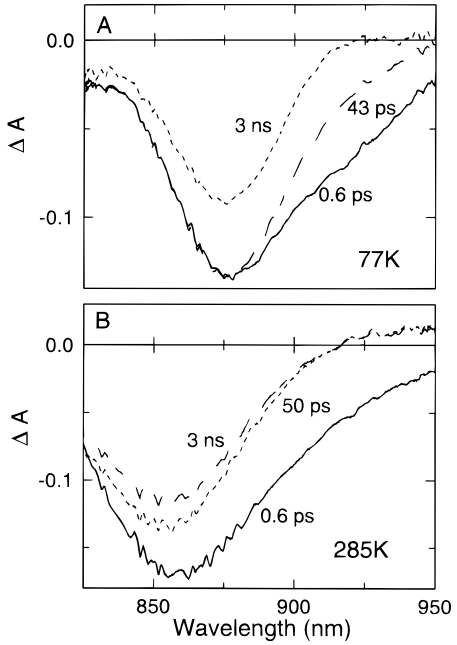

Figure 10. Representative near-infrared absorption difference spectra acquired following a 150 fs flash at 580 nm for G(M201)D/L(M212)H RCs at (A) 77 K and (B) 285 K.

The primary photochemistry of all three mutants near ambient temperature has been previously reported;[3,7] additional measurements were carried out here on the double mutant. Representative data both at 77 and 285 K for the various mutants are shown in Figures 9−12, and the resulting state lifetimes and relative yields are collected in Table 2.

It is convenient to present the results on the various RCs under a common framework. This is accomplished using the general scheme $P^* \rightarrow P^+I^- \rightarrow P^+Q_A^-$ for the charge-separation events, including the competitive decay pathways to the ground state (see Figure 3). It is important to keep in mind that P^+I^- is used generically throughout this discussion and that the detailed nature and characteristics of the intermediate so denoted differ

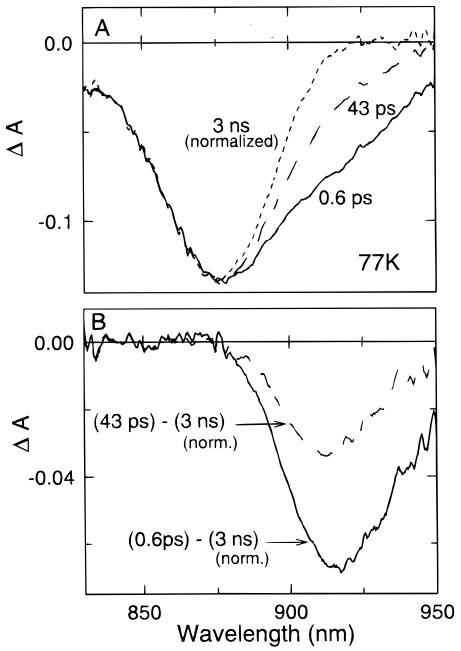

Figure 11. Spectra for the G(M201)D/L(M212)H RCs at 77 K (from Figure 10) with the spectrum at 3 ns ($P^+Q_A^-$) normalized to the amplitude of the P bleaching (840−870 nm) in the spectra at 43 and 0.6 ps (A). The spectra in (B) show the stimulated emission contribution to the spectra at 0.6 (P*) and 43 ps (P^+I^-/P* mixture).

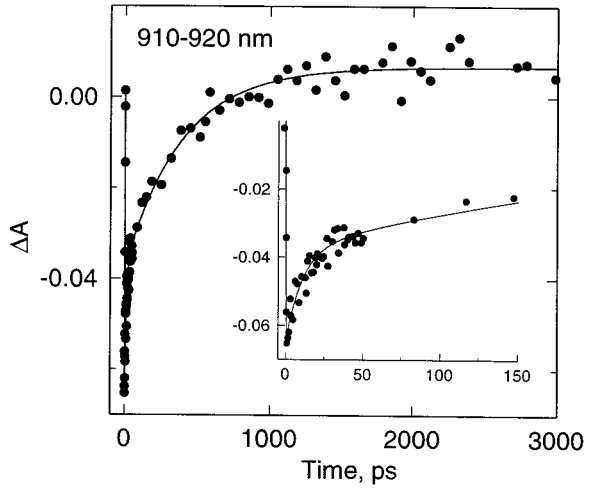

Figure 12. Time-evolution of the stimulated emission from G(M201)D/L(M212)H RCs at 77 K in the 910−920 nm region. The solid line is a computer fit of the data to a dual-exponential function with time constants of 11 ± 2 and 420 ± 60 ps. Table 2 gives the average time constants obtained in the region shown in Figure 10.

among the various RCs. For example, it is well known that P^+I^- is $P^+BPh_L^-$ for the wild-type RC (Figure 3A). The same assignment is readily made for the G(M201)D mutant due to the overall wild-type-like characteristics observed for the primary photochemistry (vide infra). On the other hand, P^+I^- is best characterized as a thermal/quantum admixture of $P^+BChl_L^-$ and $P^+\beta^-$ (due in part to their close energetic proximity) in β-containing RCs such as the L(M212)H mutant (Figure 3B).[3] To facilitate comparisons, we will first present the data for the G(M201)D and L(M212)H single mutants, followed by that for the G(M201)D/L(M212)H double mutant.

G(M201)D RCs. The photochemistry of the G(M201)D mutant at 77 K is basically wild-type in nature, as found previously for this mutant and the *Rb. sphaeroides* G(M203)D analog at room temperature.[6,7] In Figure 9A, the three spectra

TABLE 2: Observed Lifetimes and Relative Yields for Wild-Type and Mutant RCs

		P* decay		P^+I^- decay	
sample	T (K)	τ (ps)	P bleach ratio[a]	τ (ps)	P bleach ratio[a]
wild type	285	4.3 ± 0.2	1	176 ± 12	1
	77[b]	2.4 ± 0.5	1	100 ± 20	1
G(M201)D	285[c]	7.6 ± 0.5	1	159 ± 14	1
	77	10 ± 2	1		1
L(M212)H	285[c]	8.5 ± 0.8	1	212 ± 15	0.76
	77	6.5 ± 0.9	1	410 ± 60	0.76
G(M201)D/L(M212)H	285[d]	15 ± 1	0.85	170 ± 20	>0.9
	77	13 ± 3	1	470 ± 80	0.70

[a] The value listed is the amplitude (within ∼5%) of the P bleach remaining after the decay of the state relative to the initial amplitude for that state (i.e., the extent of ground-state recovery that occurs during the decay of the state is $1 - R$, where R is the P bleach ratio listed). In the absence of electron transfer via the M branch, the value listed for the P* decay is the fraction of this state that decays to P^+I^-. In the absence of repopulation of P* (or formation of other transient states), the value listed for the P^+I^- decay is the fraction of this state that decays to $P^+Q_A^-$. [b] The low-temperature values are for *Rb. sphaeroides* RCs, which at room temperature have values similar to *Rb. capsulatus* RCs at room temperature. [c] Taken from ref 7. [d] See refs 3e and 23.

correspond to the states P* (0.6 ps), P^+I^- (ie., $P^+BPh_L^-$) (51 ps), and $P^+Q_A^-$ (3 ns). The key observations include the following. (i) The P* → P^+I^- ($P^+BPh_L^-$) → $P^+Q_A^-$ processes are essentially quantitative, as reflected in the constant amplitude of the P bleaching (850−880 nm) throughout this overall conversion (see Figure 9A). (ii) The stimulated emission (880−950 nm) decays completely during the ∼10 ps P* lifetime (e.g., by ∼50 ps). Nevertheless, the G(M201)D mutation does affect the rate of the initial charge-separation event. The P* lifetime, as reflected by the decay kinetics of the stimulated emission, is somewhat longer in G(M201)D than in wild-type RCs at both 77 K (10 versus 2.4 ps) and at 285 K (7.6 versus 4.3 ps). (Similarly, the P* lifetime of 9.4 ps at room temperature for the *Rb. sphaeroides* G(M203)D analog is longer than that for wild-type RCs.[6]) Also, the P* lifetime in the G(M201)D mutant is marginally longer at 77 versus 285 K (10 versus 7.6 ps). This behavior is in contrast to that of wild-type RCs (and many mutants),[1,3d] wherein the P* lifetime becomes shorter as the temperature is reduced (Table 2).

L(M212)H RCs. The primary photochemistry observed for the L(M212)H mutant at 77 K is very similar to that previously reported for this mutant at 285 K and for other β-containing single mutants[3] (and the F(L121)D mutant[6]) at a number of temperatures. The beta-type photochemistry observed in these various RCs has been discussed in detail previously and is summarized in Figure 3B. Along these lines, the spectra shown for the L(M212)H mutant at 77 K in Figure 9B can be assigned to P* (0.6 ps), P^+I^- (thermal/quantum admixture of $P^+\beta^-$ and $P^+BChl_L^-$) (48 ps), and $P^+Q_A^-$ (3 ns). The key points regarding the low-temperature results for this mutant are as follows (Figure 9B and Table 2). (i) The yield of P* → P^+I^- is near unity, as indicated by the constant amplitude of the P bleaching (850−880 nm) during the decay of the stimulated emission (880−950 nm). (ii) The stimulated emission decays completely during the P* lifetime (compare spectra at 48 ps versus 0.6 ps). (iii) The P* lifetime becomes slightly shorter as the temperature is reduced. (iv) The P* lifetime in the L(M212)H mutant is somewhat longer than in wild-type RCs. (v) The yield of P^+I^- → $P^+Q_A^-$ is reduced to ∼75% in the L(M212)H mutant, compared to ∼100% for wild-type and G(M201)D RCs, as reflected in the decay of P bleaching in the spectra obtained at

48 ps versus 3 ns. The decay of the P bleaching occurs with a time constant of ~400 ps; the same time constant is measured in the anion region (620−700 nm; not shown).

Using a simple branching model for the decay of P^+I^- in the L(M212)H mutant (as in Figure 3B), the observed P^+I^- lifetime and the fractional P-bleaching decay (ground-state recovery) give inherent rate constants for the $P^+I^- \rightarrow$ ground state and $P^+I^- \rightarrow P^+Q_A^-$ processes of $(880\ ps)^{-1}$ and $(280\ ps)^{-1}$, respectively, at 285 K and $(1.7\ ns)^{-1}$ and $(540\ ps)^{-1}$, respectively, at 77 K. For comparison, the rate constants for the $P^+I^- \rightarrow$ ground state and $P^+I^- \rightarrow P^+Q_A^-$ processes in wild-type RCs are $(10-20\ ns)^{-1}$ and $(100-200\ ps)^{-1}$, respectively. Thus, the M(L212)H mutant at 77 K retains the same significant increase in the rate constant for P^+I^- charge recombination that is the main defining characteristic of the beta-type RCs (and the F(L121D) mutant) at ambient temperature.[3,7] This greatly enhanced back-reaction rate, together with a somewhat slower electron-transfer rate onto Q_A, gives rise to a branching in the electron-transfer pathway at the P^+I^- stage of charge separation in the M(L212)H RC and related mutants.

G(M201D/L(M212)H RCs. Unlike the modest effect of temperature on the primary photochemistry in the G(M201)D and L(M212)H single mutants, dramatic changes occur in both stages of charge separation ($P^* \rightarrow P^+I^- \rightarrow P^+Q_A^-$) in the G(M201)D/L(M212)H double mutant at 77 versus 285 K. The most notable differences are readily seen by direct inspection of the absorption difference spectra for the double mutant at the two temperatures (part A versus part B of Figure 10). The key findings at low temperature are as follows.

(i) The P* stimulated emission decay is biexponential. This apparently arises from the normal decay of state P* as well as repopulation of P* from P^+I^-. This second aspect is manifested in the time-resolved spectra by the significant contribution of stimulated emission (negative ΔA in the 880−950 nm region) that persists at 43 ps (Figure 10A) and well beyond at 77 K. To further demonstrate this point, in Figure 11A, we have normalized the 3 ns $P^+Q_A^-$ (which does not contain stimulated emission) of Figure 10A to the amplitude of the P bleaching (840−870 nm) in the spectra at 0.6 ps (due to P*, as in the single mutants in Figure 9) and at 43 ps. In Figure 11B, these spectra have been subtracted to reveal the contribution of stimulated emission in both the 0.6 ps and 43 ps spectra (differing in amplitude but not shape at the two times). Figure 12 shows a representative stimulated emission decay profile and a dual-exponential fit. The average time constants obtained across the stimulated emission region are 13 ± 3 ps (P* lifetime) and 470 ± 80 ps (nominally the P^+I^- lifetime but obviously representing decay of a P^+I^-/P* mixture). The contribution of stimulated emission to the nominal P^+I^- spectrum (i.e., at 43 ps) is not observed for G(M201)D/L(M212)H RCs at 285 K (Figure 10B) or for the L(M212)H and G(M201)D single mutants and wild-type RCs at either 77 or 285 K (see Figure 9).

(ii) There is no decay of P bleaching (~840−880 nm) during the initial ~13 ps P* lifetime (i.e., there is essentially unity yield of $P^* \rightarrow P^+I^-$), but there is a 30% decay of P bleaching at longer times (reflecting a 30% yield of $P^+I^- \rightarrow$ ground state and a 70% yield of $P^+I^- \rightarrow P^+Q_A^-$) (Figure 10A). The time constant for the decay obtained across the P-bleaching region has the same average value (~500 ps) as is found for the longer component to the stimulated emission decay (vide supra). In other words, in the simplest model, the overall photochemistry of the double mutant at 77 K is generically similar to that indicated for the beta-type single mutants in Figure 3B. This behavior is completely opposite to that which is observed for the double mutant at 285 K, where the branching of the photochemistry is as indicated in Figure 3C. At 285 K (Figure 10B), there is a 15% decay of P bleaching between the early- versus intermediate-time spectra (reflecting a corresponding reduction in the $P^* \rightarrow P^+I^-$ yield) with less than 10% decay at longer times (nearly quantitative $P^+I^- \rightarrow P^+Q_A^-$ yield).[23]

The above findings show that there is a temperature-dependent switch in whether there is a loss in the quantum yield of charge separation (as reflected in the decay of P bleaching) at P* (near ambient temperature) or P^+I^- (low temperature). At neither temperature is the overall yield of charge separation to $P^+Q_A^-$ unity as in the wild-type or the single G(M201)D mutant. Nor does the double mutant behave exactly like the β-containing single mutants (or F(L121D RCs) at any temperature. Although the branching point in the photochemistry is similar (at what is nominally P^+I^-), the large component of stimulated emission decay accompanying the P^+I^- decay in the G(M201)D/L(M212)H RCs at 77 K speaks to significant differences relative to the L(M212)H (and related) single mutants (and to the double mutant at 285 K).

Using the relative yields and P^+I^- lifetime for the G(M201)D/L(M212)H mutant at 77K, a simple branching model for the P^+I^- decay gives inherent time constants for the $P^+I^- \rightarrow$ ground state and $P^+I^- \rightarrow P^+Q_A^-$ processes of $(1.6\ ns)^{-1}$ and $(780\ ps)^{-1}$, respectively. These values are rough estimates of the actual rate constants due to the obviously close equilibrium between P* and P^+I^- (which requires a more complex model) and are presented only for comparison purposes. These modeled rate constants are very similar to those found above for the same processes in the single L(M212)H mutant at 77 K, namely $(1.7\ ns)^{-1}$ and $(540\ ps)^{-1}$, respectively. The behavior of the G(M201)D/L(M212)H and L(M212)H RCs at 77 K is also similar in the Q_x region (not shown), where a small bleaching in the region of the 530 nm ground-state band of BPh_M is observed and found to have comparable amplitude in the two mutants. This situation is quite different than that found here and previously at 285 K, in which the BPh_M bleaching is found to be over 2-fold larger in G(M201)D/L(M212)H than in L(M212)H RCs.[3e] Collectively, all of the above findings show that there is a profound temperature-dependent property associated with Asp M201 that causes a significant effect on the primary photochemistry in the double mutant.

Discussion

The replacement of Gly M201 with Asp in a mutant that also contains a BChl (β) in place of BPh_L has been shown to have significant effects on the primary photochemistry near ambient temperature.[3e] The perturbations to the rates and yields of charge-separation/recombination lead to the conclusion that state $P^+BChl_L^-$ is elevated in free energy in the G(M201)D/L(M212)H mutant relative to its position in L(M212)H and wild-type RCs (Figure 3). One possibility for this free-energy shift is that Asp M201 is ionized (negatively charged) thereby destabilizing $BChl_L^-$. In the present studies, we have found that the primary photochemistry in the G(M201)D/L(M212)H mutant also changes in significant ways at low temperature, and in a manner that implies a diminished effect of Asp M201. The RR studies reported herein were undertaken to elucidate how the incorporation of Asp M201 affects the vibrational/electronic properties of $BChl_L$, which in turn mediate the various changes in the charge-separation process. Two key questions concern the structure/conformation of $BChl_L$ and the charge/protonation of Asp M201. In the following section, we address both of these

issues. We then discuss how Asp M201 affects the primary photochemistry in the context of changes in the properties of $BChl_L$. Finally, we discuss how these properties are affected by temperature.

Properties of $BChl_L$ and Asp M201. The first important finding that emerges from the RR studies of the G(M201)D and G(M201)D/L(M212)H mutants is that replacing Gly M201 with Asp has no discernible effect on the vibrational characteristics of the ring-skeletal modes of $BChl_L$. This result by itself indicates that the structure/conformation of the electronic ground state of $BChl_L$ is unperturbed by the Asp residue. On the other hand, Asp M201 does affect certain properties of the Q_y-excited state of $BChl_L$ (as indicated by both ground-state absorption and RR intensity differences versus those of wild-type RCs).

The second important finding is that the introduction of Asp M201 causes significant frequency shifts in the $\nu C_9{=}O$ mode of $BChl_L$. The shifts of the $\nu C_9{=}O$ mode in the G(M201)D and G(M201)D/L(M212)H) RCs (each $+7$ cm^{-1}) are in the same direction but somewhat smaller than the shift observed for the $\nu C_9{=}O$ mode of BPh_L in the F(L121)D mutant ($+10$ cm^{-1}).[10] As we have previously discussed in detail, the direction of the RR shift observed for the $\nu C_9{=}O$ mode of BPh_L in the F(L121)D RCs, in conjunction with the relative orientation of the Asp L121 residue with respect to ring V, leads to the assessment that Asp L121 is deprotonated and negatively charged.[10] As is discussed below, similar arguments strongly suggest that Asp M201 is also deprotonated. The difference in the magnitude of the effects of Asp M201 versus Asp L121 on the $\nu C_9{=}O$ mode of $BChl_L$ versus BPh_L may reflect differences in either the location (such as above versus in the plane of the ring) or the distance/orientation of the Asp with respect to ring V of the cofactor, or differences in the local dielectric environments (e.g., due to the presence of water molecules).

The assessment that Asp M201 is deprotonated and negatively charged is based on the following considerations. If this residue were instead protonated and neutral, the predominant interaction between the carboxyl group of the Asp and the C_9-keto group of $BChl_L$ would be dipole−dipole in nature. The dipole moment of the C_9-keto group lies along the carbon−oxygen bond vector, whereas that of the Asp carboxyl lies approximately along the bisector of this group, regardless of the protonation/charge state of the Asp. This latter bond vector is approximately orthogonal to the carbon−oxygen bond vector of the C_9-keto group (Figure 4, right panel). This angle is obtained under the reasonable assumption that the torsional conformation of the methylene group of Asp M201 is such that the carboxyl residue points generally towards the C_9-keto group rather than the C_{10a}-carbomethoxy group. The near orthogonality of the dipole moments of the Asp carboxyl and C_9-keto groups minimizes the dipole−dipole interaction. Accordingly, the latter type of interaction cannot account for the upshift of the $\nu C_9{=}O$ mode in the two Asp M201 mutants. It should also be noted that the upshift of the $\nu C_9{=}O$ vibration is incompatible with hydrogen bonding to the C_9-keto group. Hydrogen bonding generally lowers the frequency of $\nu C{=}O$ modes.[12a,20] [Furthermore, the absolute position of the RR band in either wild-type RCs or the mutants containing Asp M201 are inconsistent with hydrogen bonding to the $\nu C_9{=}O$ group of $BChl_L$ (by Asp M201 or other species such as water molecules[21]).] On the other hand, a relatively nonspecific charge−dipole interaction between the carboxyl group of a deprotonated, negatively charged Asp M201 and the C_9-keto group of $BChl_L$ would tend to destabilize $C_9^{+}{-}O^{-}$ and all other charge-separated resonance forms. The destabilization of these resonance forms would tend to *upshift* the $\nu C_9{=}O$ mode of $BChl_L$ owing to slightly enhanced double-bond character. This picture is entirely consistent with the observed RR data for both the G(M201)D and G(M201)D/L(M212)H RCs. As noted above, this same picture is entirely consistent with the previously observed *upshift* in the $\nu C_9{=}O$ mode of BPh_L in the F(L121)D mutant.[10]

Effect of Asp M201 on the Primary Photochemistry near Ambient Temperature. The assessment that Asp M201 (near ring V of $BChl_L$) is deprotonated and negatively charged provides a unifying and self-consistent molecular framework for understanding the perturbations to both the electronic/vibrational properties of $BChl_L$ and the primary photochemistry in RCs containing the G(M201)D mutation. We have made a similar assessment concerning the ionization state of Asp L121 (near ring V of BPh_L) from analysis of the properties of BPh_L and the electron-transfer characteristics in F(L121)D RCs.[3e,7,10] Collectively, the strong correlations that exist among the properties and various effects of Asp residues placed near $BChl_L$ and BPh_L make a compelling case for the validity of the general conclusions that have emerged from these studies.

As noted above, one such conclusion is that incorporation of Asp M201 perturbs the reduction potential of $BChl_L$, thereby raising $P^{+}BChl_L^{-}$ in free energy from slightly below P* to slightly above (a shift of 100 meV or more).[3e] The consequences on the primary photochemistry are dramatic in the G(M201)D/L(M212)H double mutant, which also contains a BChl (denoted β) in place of BPh_L. These multiple effects include a switch in the predominant branching point in the photochemistry from $P^{+}I^{-}$ to P* that involves the following specific aspects (Figure 3). (1) There is a diminished involvement of $P^{+}BChl_L^{-}$ in the formation of $P^{+}\beta^{-}$ relative to the L(M212)H single mutant (probably involving both the one- and two-step mechanisms[3e,7]). This effect contributes (along with the replacement of BPh_L with β) to a lengthening of the P* lifetime, allowing competitive decay to the ground state and increased electron transfer to BPh_M to be observed in the double mutant. (2) There is a diminished contribution of $P^{+}BChl_L^{-}$ to the decay properties of $P^{+}\beta^{-}$. In the double mutant, the free-energy gap between these states is closer to that between $P^{+}BChl_L^{-}$ and $P^{+}BPh_L^{-}$ in wild-type RCs due to the greater free energy of $P^{+}BChl_L^{-}$. The consequence is that the rates and yields of increased electron transfer to Q_A and charge recombination to the ground state return closer to those characteristic of $P^{+}BPh_L^{-}$ in wild-type RCs (Figure 3).

Although less dramatic perturbations of the primary photochemistry are found upon the incorporation of Asp M201 in the wild-type background, the results on the G(M201)D single mutant are also fully consistent with the same effect of the Asp to increase the free energy of $P^{+}BChl_L^{-}$. In particular, the longer P* lifetime in the G(M201)D versus wild-type RCs (7.6 versus 4.3 ps at 285 K) can be ascribed to a diminished contribution of $P^{+}BChl_L^{-}$ to formation of $P^{+}BPh_L^{-}$. The fact that the P* lifetime and its decay pathways are not as substantially perturbed in the G(M201)D RC as in the G(M201)D/L(M212)H RC follows because the single mutant retains BPh_L whereas in the double mutant, this cofactor is replaced with β. The associated consequence that $P^{+}BPh_L^{-}$ in the G(M201)D mutant should be unperturbed relative to wild-type RC underlies the finding that the decay properties of this state are also essentially the same in these two RCs. In particular, $P^{+}BChl_L^{-}$ in wild-type RCs already lies sufficiently above $P^{+}BPh_L^{-}$ in wild-type RCs so that the effect of the free-energy upshift of $P^{+}BChl_L^{-}$ in the G(M201)D single mutant is only to further diminish any contribution of this state to the decay properties of $P^{+}BPh_L^{-}$.

Because electron transfer to Q_A is already essentially quantitative in wild-type RCs, one observes little change in the charge-separation process in the M(G201)D mutant.

Temperature Dependence of the Effects of Asp M201. A reduction in temperature causes clear and significant effects on specific electronic/vibrational characteristics of $BChl_L$ in the G(M201)D and G(M201)D/L(M212)H RCs and the photochemistry in the double mutant. Consider first the effects of Asp M201 on the νC_9=O mode of $BChl_L$. As the temperature is reduced, the intensity of this mode is significantly diminished relative to room temperature causing the band contour in the associated region of the RR spectrum of the G(M201)D and G(M201)D/L(M212)H mutants to become much more like that observed for wild-type RCs (Figure 8). Given all the considerations discussed above, this result implies that the interaction between Asp M201 and $BChl_L$ that serves to modulate the properties of the νC_9=O mode at room temperature is changed (diminished) at low temperature. However, two additional aspects are especially noteworthy in assessing the molecular origin of this temperature effect. (1) The frequency of the νC_9=O mode of $BChl_L$ does not change significantly (by a few wave numbers or less) with temperature. This finding implies that a reduction in temperature does result in a quantitative change in the protonation/charge state of Asp M201. However, we cannot exclude the possibility that Asp M201 is protonated in some fraction of the RCs at low temperature. (2) The ring-skeletal vibrations of $BChl_L$ are essentially unchanged with temperature, implying that a significant change in the structure/conformation of this cofactor is not responsible for the temperature dependence of the νC_9=O mode in the G(M201)D-containing RCs. Collectively, these findings indicate that the apparent diminution of the interaction between the carboxyl group of Asp M201 and the νC_9=O group of $BChl_L$ as the temperature is reduced derives from several factors. These include a change in the dielectric environment of Asp M201/$BChl_L$ (perhaps involving a water molecule present in the site[2a]) or the distance/orientation between the two groups (perhaps involving in part the shallow torsional potentials involved). Such factors would modulate the charge/dipole interaction between the respective groups and thereby affect the specific vibrations involved.

This same reasoning, when coupled with the ideas described above concerning the effect of Asp M201 to raise the free energy of $P^+BChl_L^-$ near ambient temperature, provides a basis for understanding the significant temperature effect on the photochemistry in the G(M201)D/L(M212)H mutant and the lesser but noteworthy effects on the G(M201)D single mutant. In particular, a diminished interaction between Asp M201 and $BChl_L$ at low temperature would cause the free energy of $P^+BChl_L^-$ to decrease relative to the situation at room temperature, namely to return toward the wild-type position. Since a consistent explanation of the photochemistry near room temperature is obtained if $P^+BChl_L^-$ lies slightly above P* in the G(M201)D-containing mutants compared to slightly below P* in wild-type RCs (the states are probably within 100 meV or so in both cases),[3e,7] it follows that $P^+BChl_L^-$ must be essentially isoenergetic with P* in the mutants at low temperature.

A diminished effect of Asp M201 and the consequent lower free energy of $P^+BChl_L^-$ in the G(M201)D/L(M212)H at low temperature would tend to reverse some of the effects that the incorporation of Asp M201 has on the primary photochemistry relative to the L(M212)H single mutant (see parts B and C of Figure 3). Specifically, the branching of the photochemistry (deactivation versus charge separation) would decrease at the P* stage and increase at the P^+I^- stage, making the lifetimes and yields appear more "beta-like", as is observed (Table 2). Furthermore, the finding that the stimulated emission from P* has a second component (in addition to the fast component due to the initial decay of P*) with a time constant of about 500 ps at low temperature is fully consistent with the idea that the free energy of $P^+BChl_L^-$ drops to closer to (or nearly isoenergetic with) P*. This situation would facilitate thermal repopulation of P* from P^+I^- (which itself is a thermal/quantum admixture of $P^+BChl_L^-$ and $P^+\beta^-$ in the L(M212)H RCs). The result would be "delayed" stimulated P* emission occurring with the same P^+I^- lifetime as found in other spectral regions, as is observed. For reasons analogous to those outlined above, there are only small effects of temperature on the primary photochemistry in the G(M201)D mutant (including a slightly *longer* P* lifetime at 77 K; Table 2) that are entirely consistent with results and interpretations for the G(M201)D/L(M212)H mutant.

The effects of temperature on the primary photochemistry in wild-type RCs and many mutants has been exploited to obtain useful information on the mechanisms of electron transfer and the free energies between the states in the RC. However, the results obtained here suggest that, at least in some mutants, temperature can have significant effects that derive from changes in pigment/protein interactions and that do not simply result from a change in kT and consequent thermal population effects. In particular, it seems clear that the temperature dependence of specific vibrational properties of $BChl_L$ and of many aspects of the primary photochemistry in the G(M201)D/L(M212)H RCs derives from a change in the interaction between Asp M201 and $BChl_L$. Thus, attempts to model the temperature dependence of the rates and yields of electron transfer in the G(M201)D/L(M212)H mutant in terms of simple changes in the thermal repopulation of one state from another would prove futile. Similarly, we have previously found that for a variety of mutants, simple thermal equilibrium models and changes in kT cannot explain the effects of temperature on the various stages of charge separation when analyzed as a collective whole. These previous analyses require the assumption that multiple inherent rate constants and perhaps free-energy gaps change with temperature. The simple β-containing RCs are prime examples.[3d] The temperature dependence of individual reactions in isolation can be analyzed and energy gaps, for example, extracted, but the meaning of the results is uncertain.

Conclusions

The incorporation of an Asp residue at position M201 in the bacterial RC has dramatic consequences on the electronic/vibrational properties of the nearby $BChl_L$ cofactor and on the photochemistry in RCs containing this mutation along with the replacement of BPh_L with a BChl (β). A consistent assessment of all these properties is obtained if Asp M201 is deprotonated and negatively charged, thereby modulating the characteristics of the νC_9=O vibration of $BChl_L$, the redox potential of this cofactor, and the free energy of state $P^+BChl_L^-$. Finally, the interaction between Asp M201 and $BChl_L$ and the salient associated properties are dependent on temperature, further demonstrating that the effects of temperature on the properties of RCs may not simply derive from changes in the available thermal energy.

Acknowledgment. This work was supported by Grant GM-39781 (D.F.B.) from the National Institute of General Medical Sciences and Grant MCB-9723008 from the National Science Foundation (C.K. and D.H.).

References and Notes

(1) (a) *The Photosynthetic Reaction Center*; Deisenhofer, J., Norris, J. R., Eds.; Academic: San Diego, CA, 1993; Vol. II. (b) *Anoxygenic Photosynthetic Bacteria*; Blankenship, R. E., Madigan, M. T., Bauer, C. E., Eds.; Kluwer Academic Publishers: Dordrect, The Netherlands, 1995; pp 503−708. (c) *The Reaction Center of Photosynthetic Bacteria*; Michel-Beyerle, M. E., Ed.; Springer: Berlin-Heidelberg, 1996.

(2) (a) Ermler, U.; Fritzsch, G.; Buchanan, S.; Michel, H. *Structure* **1994**, *2*, 925−936. (b) Deisenhofer, J.; Epp, O.; Sinning, I.; Michel, H. *J. Mol. Biol.* **1995**, *246*, 429−457. (c) Yeates, T. O.; Komiya, H.; Chirino, A.; Rees, D. C.; Allen, J. P.; Feher, G. *Proc. Natl. Acad Sci. U.S.A.* **1988**, *85*, 7993−7997. (d) El-Kabbani, O.; Chang, C.-H.; Tiede, D.; Norris, J.; Schiffer, M. *Biochemistry* **1991**, *30*, 5361−5369.

(3) (a) Kirmaier, C.; Gaul, D.; DeBey, R.; Holten, D.; Schenck, C. C. *Science* **1991**, *251*, 922−927. (b) Heller, B. A.; Holten, D.; Kirmaier, C. *Biochemistry* **1995**, *34*, 5294−5302. (c) Kirmaier, C.; Laporte, L.; Schenck, C. C.; Holten, D. *J. Phys. Chem.* **1995**, *99*, 8903−8909. (d) Kirmaier, C.; Laporte, L.; Schenck, C. C.; Holten, D. *J. Phys. Chem.* **1995**, *99*, 8910−8917. (e) Heller, B. A.; Holten, D.; Kirmaier, C. *Science* **1995**, *269*, 940−945.

(4) (a) Scheer, H.; Gartwich, G. *Anoxygenic Photosynthetic Bacteria*; Blankenship, R. E., Madigan, M. T., Bauer, C. E., Eds.; Kluwer Academic Publishers: Dordrecht, The Netherlands, 1995; pp 649−663. (b) Shkurapatov, A.Y.; Shuvalov, V. A. *FEBS Lett.* **1993**, *322*, 168−172. (c) Schmidt, S.; Arlt, T.; Hamm, P.; Huber, H.; Nagele, T.; Wachtveitl, J.; Meyer, M.; Scheer, H.; Zinth, W. *Chem. Phys. Lett.* **1994**, *223*, 116−120. (d) Huber, H.; Meyer, M.; Nagel, T.; Hartl, I.; Scheer, H.; Zinth, W.; Wachtveitl, J. *Chem. Phys.* **1995**, *197*, 297−305.

(5) Felton, R. H. In *The Porphyrins*; Dolphin, D., Ed.; Academic: New York, 1978; Vol. V, pp 53−126.

(6) Williams, J. C.; Alden, R. H.; Murchison, H. A.; Peloquin, J. M.; Woodbury, N. W.; Allen, J. P. *Biochemistry* **1992**, *31*, 11029−11037.

(7) Heller, B. A.; Holten, D.; Kirmaier, C. *Biochemistry* **1996**, *35*, 15418−15427.

(8) Bylina, E. J.; Kirmaier, C.; McDowell, L. M.; Holten, D.; Youvan, D. C. *Nature* **1988**, *336*, 182−184.

(9) Lin, X.; Murchison, H. A.; Nagarajan, V.; Parson, W. W.; Allen, J. P.; Williams, J. C. *Proc. Natl. Acad. Sci. U.S.A.* **1994**, *91*, 10265−10269.

(10) Cua, A.; Kirmaier, C.; Holten, D.; Bocian, D. F. *Biochemistry* **1998**, *37*, 6394−6401.

(11) For a review, see: Lutz, M. *Biospectrosc.* **1995**, *1*, 313−327.

(12) (a) Palaniappan, V.; Martin, P. C.; Chynwat, V.; Frank, H. A.; Bocian, D. F. *J. Am. Chem. Soc.* **1993**, *115*, 12035−12049. (b) Palaniappan, V.; Schenck, C. C.; Bocian, D. F. *J. Phys. Chem.* **1995**, *99*, 17049−17058. (c) Laporte, L. L.; Palaniappan, V.; Davis, D. G.; Kirmaier, C.; Schenck, C. C.; Holten, D.; Bocian, D. F. *J. Phys. Chem.* **1996**, *44*, 17696−17707. (d) Czarnecki, K; Diers, J. R.; Chynwat, V.; Erickson, J. P.; Frank, H. A.; Bocian, D. F. *J. Am. Chem. Soc.* **1997**, *119*, 415−426. (e) Czarnecki, K.; Chynwat, V.; Erickson, J. P.; Frank, H. A.; Bocian, D. F. *J. Am. Chem Soc.* **1997**, *119*, 2594−2595. (f) Czarnecki, K.; Schenck, C. C.; Bocian, D. F. *Biochemistry* **1997**, *36*, 14697−14704.

(13) (a) Cherepy, N. J.; Shreve, A. P.; Moore, L. J.; Franzen, S.; Boxer, S. G.; Mathies, R. A. *J. Phys. Chem.* **1994**, *98*, 6023−6029. (b) Cherepy, N. J.; Holzwarth, A.; Mathies, R. A. *Biochemistry* **1995**, *34*, 5288−5293. (c) Cherey, N. J.; Shreve, A. P.; Moore, L. J.; Boxer, S. G.; Mathies, R. A. *J. Phys. Chem B* **1997**, *101*, 3250−3260. (d) Cherepy, J. M.; Shreve, A. P.; Moore, L. J.; Boxer, S. G.; Mathies, R. A. *Biochemistry* **1997**, *36*, 8559−8566.

(14) Yu, N.-T.; Srivastava, R. B. *J. Raman Spectrosc.* **1980**, *9*, 166−171.

(15) Diers, J. R.; Bocian, D. F. *J. Am. Chem. Soc.* **1995**, *117*, 6629−6630.

(16) Shreve, A. P.; Cherepy, N. J.; Mathies, R. A. *Appl. Spectrosc.* **1992**, *46*, 707−711.

(17) Kirmaier, C.; Holten, D. *Biochemistry* **1991**, *30*, 609−613.

(18) In ref 12a, we suggest that the 1700 cm^{-1} band observed with λ_{ex} = 800 nm could be due to a νC_9═O mode of P_M. However, more recent sudies[10,12f] suggest that a more likely assignment is to a combination band.

(19) (a) Peloquin, J. M.; Bylina, E. J.; Youvan, D. C.; Bocian, D. F. *Biochemistry* **1990**, *29*, 8417−8424. (b) Palaniappan, V.; Bocian, D. F. *Biochemistry* **1995**, *34*, 11106−11116.

(20) (a) Lutz, M.; Robert, B. In *Biological Applications of Raman Spectroscopy*; Spiro, T. G., Ed.; Wiley: New York, 1988; Vol. 3, pp 347−411. (b) Lutz, M.; Mäntele, W. In *Chlorophylls*; Scheer, H., Ed.; CRC Press: Boca Raton, FL, 1991; pp 855−902.

(21) The X-ray crystal structure of Rb. sphaeroides shows water molecules in close proximity to the C_9-keto groups of $BChl_{L,M}$.[2a] As a consequence, it has been suggested that these water molecules are hydrogen bonded to the C_9-keto groups of both cofactors. Regardless, the vibrational signatures for the νC_9═O modes are not commensurate with the formation of hydrogen bonds.[12a,20] In particular, the vibrational frequencies of the νC_9═O modes of $BChl_{L,M}$ are very similar to those of isolated BChl in a low dielectric, non-hydrogen-bonding solvent.

(22) Donohoe, R. J.; Frank, H. A.; Bocian, D. F. *Photochem. Photobiol.* **1988**, *48*, 531−537.

(23) The 285 K data on the double mutant shown in Figure 10B show a slightly larger decay between ∼50 ps and 3 ns than was reported previously[3e] between ∼50 ps and 2 ns. This difference, and the general decay on this time scale, result largely from charge recombination of the M-side state $P^+H_M^-$ (with a time constant of roughly 1−2 ns that also can be seen in other spectral regions). This process occurs in parallel with the decay processes of the L-side state P^+I^-, which allows us to place only approximate limits on the extent to which P^+I^- deactivates to the ground state (≤10%) in competition with formation of $P^+Q_A^-$ (≥90%). These issues will be discussed more fully in a forthcoming publication.